Photonic nanojet mediated backaction of dielectric microparticles

Yu-Xuan Ren[†,#], Xinglin Zeng[†,‡,#], Lei-Ming Zhou[§,#], Cihang Kong[†,||], Huade Mao[†], Cheng-Wei Qiu[§,*], Kevin K. Tsia[†,*], Kenneth K. Y. Wong[†,*]

†Department of Electrical and Electronic Engineering, The University of Hong Kong, Hong Kong SAR, China;

‡Max-Planck Institute for the Science of Light, Staudtstraße 2, 91058 Erlangen, Germany;

§Department of Electrical and Computer Engineering, National University of Singapore, Singapore 117583, Singapore.

||Department of Physics, University of Bielefeld, Universitätsstraße, 25, 33615 Bielefeld, Germany.

# These authors made equal contribution.

* Correspondence: C.Q. (chengwei.qiu@nus.edu.sg); K. T. (tsia@hku.hk); K. W. (kywong@eee.hku.hk)

ABSTRACT: Optical radiation force points to the same direction as the photon flux, while the direction reversal is quite challenging and necessitates special efforts. Herein, we present the observation of a photonic nanojet mediated backaction of dielectric particles owing to the local heating of solvent molecules inside the nanojet in a purely dielectric system. Such backaction has been verified to be photothermal, without the influence from thermally induced turbulence. Our findings have been theoretically corroborated by statistical analysis on the size-dependent force and speed. In addition to the increase with laser power, the backaction force is competing effect between the absorption and thermal conductivity of the immersion medium, and also affected by the photothermally raised background temperature. The backaction force exerts on dielectric particles with a broad size range. Since most biological particles are dielectric with a refractive index greater than that for the surrounding medium, this work could inspire applications in biophotonics, such as cell sorting and classification.

KEYWORDS: Optical manipulation, Backaction force, Photonics nanojet, Negative optical force, Dielectric particle

Introduction

Remote control in space was once a myth, but the advances in experimental modern physics demonstrates that light can manipulate objects of size spanning from tens of microns to a few nanometers, including live cells, nanoparticles, biomacromolecules, and atoms[1-3]. Since Ashkin's pioneering work on radiation pressure, the atom cooling using radiation pressure and optical tweezers with optical gradient force have become popular tools in various applications, including Bose-Einstein condensates, opto-mechanics, colloidal physics and single-molecule biophysics[4-8]. The optical manipulation has been a noncontact, indispensable, noninvasive tool to grasp and transport objects. Notably, the optical gradient force draws the particle to the intensity maximum, and can be applied to measure the force and displacement with high precision in material sciences and single molecule studies[2,3,9]. The radiation pressure produces optical pushing force ('positive force') thanks to the photon momentum conservation and transfer to the absorbing particle. Such pushing force is sufficient to balance the particle's gravitational force for all optical levitation[10].

Interestingly, by control over the topology of ambient medium, beam phase (polarization), the liquid-air interface, or the electromagnetic multipole interaction, the direction of the optical force could be reversed, producing optical pulling force which drags the particle towards the light source[11-17]. Such negative optical force (NOF, opposed to the photon flux) originates from the enhanced forward scattering[11,12,15,18,19]. For Rayleigh particles, once the light excites multipoles in the particle, the interference of the radiation multipoles would maximize the forward scattering and produce NOF[13]. Wavefront engineering was able to shape the phase gradient and control the particle motion direction and trajectory[14,20,21]. Experimental observation of NOF covered a broad spectrum including the evanescently enhanced plasmonic plates[22,23], and plasmonic nanostructure augmented backaction of dielectric nanoparticles[24]. The NOF also exists in gradient-less beam, e.g., the propagation invariant Bessel beam[13,25]. Particles in the interference region of two beams exhibit variant magnitude and opposite direction depending on the particle size[26]. The wavefront shaping relies on high precision spatial light modulator and fine computer control. For interferometric scheme, the NOF only takes place within a narrow interference region. The non-diffracting beams with zero intensity gradient, e.g., Bessel beams, however, provides limited trapping region[25]. For resonant optical force associated with the optical modes, not only the trapping region is confined, but also the interference of trapped particle breaks the electromagnetic field[15,16,23,24]. Apart from the scattering force and gradient force, the photophoretic force originates from the imbalanced heating of local molecules in close proximity to the particle surface [27,28]. Although the origin might differ slightly (thermal accommodation or temperature difference), the photophoretic force is mainly categorized into forward ('pushing') and backward ('pulling') forces[23,27,28]. The magnitude of force depends on the absorption of light energy by local molecules and the temperature distribution near the

particle surface, which can be much larger than the pure optical force.

The optical force relies on high-numerical aperture (NA) lens to concentrate the light energy at a narrow location to augment the intensity field (gradient)[9,21,29]. The dielectric microsphere assumes a spherical geometry, and is able to concentrate the light energy to form a photonic nanojet (PNJ) in the absence of high-NA objective lens [30]. Such phenomenon has been applied in optical microscope for super resolved imaging beyond the optical diffraction limit [31]. Inspired by the fluid jet mediated backaction of natural creatures, hereby, we take advantage of the PNJ to induce backaction of dielectric microspheres passively in strong absorbing medium. In contradistinction to optical force generated with objective lens of high NA, the PNJ comes innately with each microsphere provided that the sphere is exposed in the collimated light field, our observation provides a large-scale manipulation of dielectric particles without geometric restriction in contrast to the narrow trap region in traditional optical tweezers settings.

Results

Mechanism of passive backaction force

In nanophotonics, the spherical microparticle concentrates the light into a focal region, producing PNJ (see schematics in Fig. 1a) [30,31]. In brief, the PNJ features with a narrow, high-intensity, non-evanescent light field that propagates over a distance larger than light wavelength (Fig. 1b)[30,32,33]. The light energy concentrates in the PNJ, which has been demonstrated for nano-fabrication, molecular detection, all optical switching, and super-resolution label-free optical imaging[31,34-36]. In particular, the microsphere-assisted microscopy breaks the diffraction limit with resolution down to ~50 nm[31,33,37].

Newton's third law of motion states that when one object exerts a force on a second object, the second object simultaneously exerts a force opposite in direction and equal in magnitude on the first. Natural creature, like octopus, ejects a certain amount of fluid, and gains backward force, which drives the creature motion. Similarly, artificial rocket accumulates supersonic speed due to active ejection of the propellant. Due to the momentum conservation, the propellant exerts a force with opposite direction on the rocket such that the speed of the rocket increases. The speed increase of both the natural and artificial creatures relies on the active ejection of the fluidic jet, and thus the backward momentum. Hereby, we take advantage of the high concentrating ability of microsphere and the strong absorptive medium in the mid-infrared spectrum to produce a passive backaction force on the dielectric microparticle. The fluid (gas, liquid) molecules inside the concentrated region absorb the photonic energy and experience temperature rise. The molecules with escalating temperature expand and push the microsphere backwards. In contrast to previous experiments using high NA objective, the self-induced backaction takes advantage of microsphere itself to concentrate the light energy, producing a passive pulling platform.

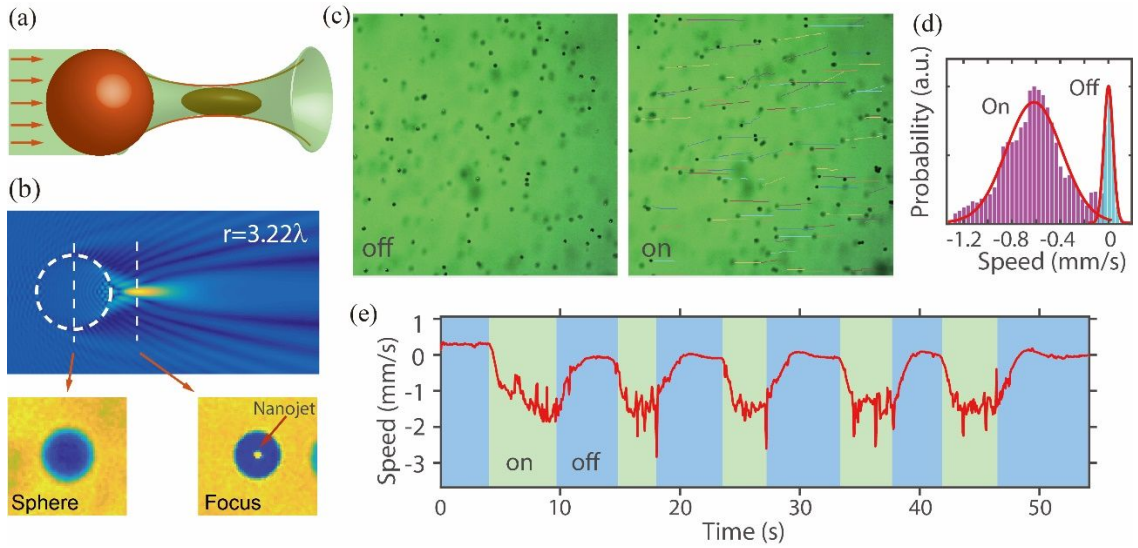

Figure 1. Photonic nanojet mediated backaction force. (a) Dielectric microsphere focuses the light into a PNJ and gain a passive backaction force. (b) Side-view electromagnetic field distribution of the PNJ formed by focusing light with microspheres. Insets show the microscopic images of microsphere and the PNJ. The radius of microsphere is labeled in the unit of wavelength. (c) Microsphere motion trajectories in the absence (left) and the presence (right) of the laser beam. Curves accompanying each particle demonstrated the motion trajectory. (d) The average backaction speed distribution with laser beam in the presence (on) and the absence (off) of the pulsed laser. (e) the magnitude of average motion speed as function of time under alternating laser beam.

The self-induced backaction on dielectric microparticles was observed by illumination using a custom-built mode-locked fiber laser with spectrum centered at 1576 nm with a repetition rate of 44.5 MHz and pulse width of ~1.6 ps (See Methods and Supplemental material). The motivation to use an ultrafast mode-locked fiber laser was the high peak power, e.g., 14 kW at an amplified average power of 1W. The observation microscope is mounted orthogonal to the mode-locked laser beam akin to the light-sheet fluorescence microscopy[38]. In the absence of laser beam, the particles experience random Brownian motion with zero average speed (left, Fig. 1c), while the speed increases to a constant value pulling the particle towards the light source in presence of plane wave pulsed laser (right, Fig. 1c). The motion

trajectory for particles with (without) laser beam is directional (random) (Fig. 1c). In the absence of laser, the velocity follows normal distribution centered at zero, while in the presence of the laser, the velocity histogram shifts to the left (Fig. 1d, Supplementary video). As we alternate the laser beam, the average speed for particles under video microscopy exhibits two states (Fig. 1e).

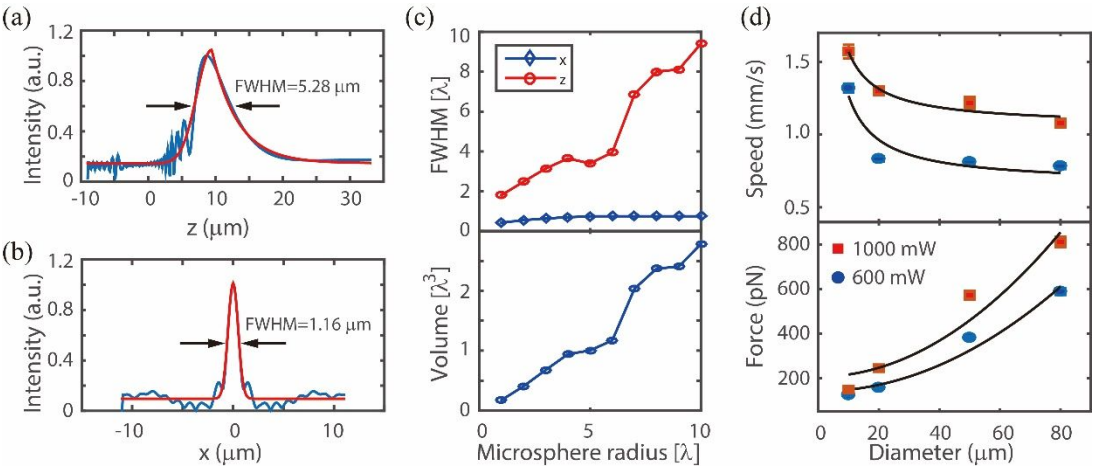

Figure 2. Geometry of PNJ and the magnitude of backaction force and speed. (a) Linear intensity profile of the nanojet along longitudinal direction. (b) Linear intensity profile of the nanojet along transverse direction. (c) The geometric size (top) and the volume (bottom) of the PNJ as function of microsphere size. (d) The speed and force as function of particle size at power levels of 600 mW and 1000 mW.

At steady state, the laser beam produced force is balanced by the fluidic drag force, thus the back-action force reads, $F = 6\pi\eta r v$, with η the viscosity of fluid, r and v are the radius and speed of particle. As the laser power ramps up, the particle speed and thus the force increases with power. The back-action force for a $10\,\mu m$ polystyrene particle is ~100 pN for a power of 1W. The magnitude of force is significantly greater than the forces originated from optical scattering, photophoresis, and thermophoresis (see Supplementary Materials). Notably, the optical scattering force at the same setting will be ~0.16 pN, which tends to push the particles away from the light source.

The microscopic image shows a clear spherical shape at the center of the microparticle, while a pronounced high intensity peak appears at the focus of the microsphere (inset in Fig. 1b). To further understand the mechanism, we evaluate the size of the PNJ using FDTD simulation (Lumerical Inc.). As the light is focused by the microsphere creating a PNJ at the shadow side of the microsphere (Fig. 1b, supplementary Fig. S1), we define each dimension as the full width at the $1/e^2$ times the maximum intensity and approximate the focus as an ellipsoid. We assume the semiaxes for nanojet are $\beta_x r$, $\beta_y r$, and $\beta_z r$ respectively, with $\beta_i\,(i = x,y,z)$ the size relative to the microsphere radius. Accordingly, the nanojet volume V_f can be defined as $V_{jet} = (4\pi/3)\beta_x\beta_y\beta_z r^3$. The PNJ formed with 10 μm diameter polystyrene microsphere with 1.55 um wavelength suggests $\beta_x = \beta_y = 0.128$, $\beta_z = 1.2$, such that the volume of PNJ is only 2% of that for microsphere, i.e., $V_{jet} = 0.02V_{sph}$ (Fig. 2a and 2b). The geometry and volume of PNJ scales up with the diameter of the microsphere (Fig. 2c).

Molecules inside the PNJ absorb strong light energy and encounter temperature rise. According to equipartition theory, the kinetic energy of the molecule is associated with the thermal energy, $(1/2)m_{sol}v^2 = (1/2)k_B T$, where m_{sol} is the mass of a solvent molecule, v is the velocity of the molecule, k_B is the Boltzmann constant, and T is the local temperature. The momentum change for each water molecule is given by, $\Delta P = (1/2)m_{sol}\Delta v$, where the constant $1/2$ statistically accounts for the probability of forward or backward motions. Assume the PNJ heats up the liquid molecules in the focal volume from temperature T_0 to T. Therefore, the backward force the microsphere experienced from the PNJ would be $F = N\Delta P/\tau$, which reads,

$$F = \frac{V_{jet}\rho_{sol}}{2\tau}\sqrt{\frac{N_A k_B}{M_{sol}}}\left(\sqrt{T} - \sqrt{T_0}\right) \qquad (1)$$

where τ characterizes the time for microspheres to respond to light, N_A is Avogadro constant, N is the total number of solvent molecules in the photonic nanojet volume V_{jet}. Assume the temperature rises from $T_0 = 298K$ to $T = 305K$, the PNJ induced optical force is $F = 138pN$, the magnitude of which is consistent with our experimental observation for $10\mu m$ polystyrene particle with an incident power of 1W [Fig. 2(d) and Supplementary Materials].

Observation of self-induced optical backaction

The PNJ mediated backaction has been observed on particles with volume spanning seven orders of magnitude from pL to tens of μL. This is corroborated by the observation that the polystyrene sphere with a diameter of a few millimeter moves towards the light in response to the light exposure (see Supplementary video). To corroborate our theory, we further analyze the dependence of force and speed on particle size. The temperature rise is usually much smaller than the room temperature, i.e., $\Delta T = T - T_0 \ll T_0$, and is proportional to the incident laser dosage divided by the volume of the PNJ, i.e., $\Delta T \propto \pi r^2 I/V_{jet}$, where I is the average intensity (power density). The PNJ induced force scales up with the square of the microsphere size, i.e., $F \propto r^2$, while the particle speed is inversely proportional to the size, i.e., $v \propto 1/r$ (see

Supplementary Materials). Figure 2(d) presents the measured particle speed and force as function of particle size with average laser power at two different levels. Solid lines well fit our hypothesis on the size dependence of the optical force and speed.

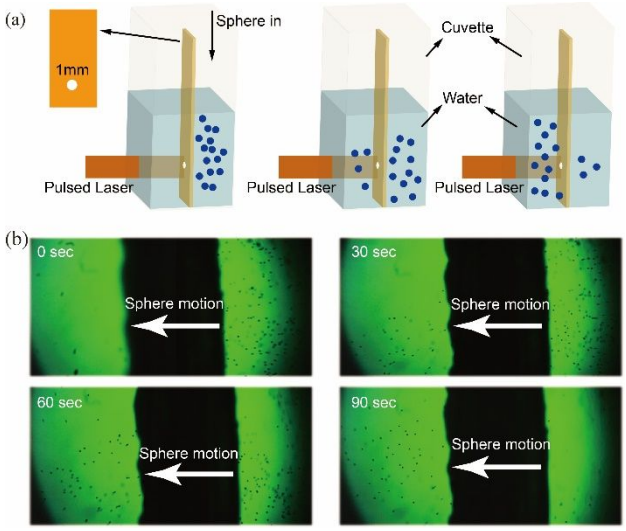

Figure 3 Isolation of the fluid turbulence. (a), The cuvette is separated into two halves by a plastic sheet (thickness ~1 mm) with an opening of diameter ~ 1 mm. Particles injected at the far side will be attracted to the beam source via the opening. (b), Snapshots from a video demonstrate the particle density decreases (increases) at the far (near) side owing to the backaction force.

We noticed that water has pronounced absorption to the studied wavelength at 1.57 μm. The light intensity decreases with propagation distance, creating an intensity gradient along beam direction. Such intensity gradient force could pull the particle towards the laser source. Unfortunately, this possible mechanism contradicts with the experimental observation. Assume the light intensity decreases with distance in the suspension, $I = I_0 \exp(-\beta z)$, with β and z the absorption coefficient and propagation distance respectively, I_0 the power density at the entrance. The magnitude of the intensity gradient force, $F = \alpha \nabla I = \alpha \beta I$, with $\alpha = 4\pi a^3(\varepsilon_p - \varepsilon_m)/(\varepsilon_p + \varepsilon_m)$ the polarizability, ε_p and ε_m the dielectric constant of particle and medium, is proportional to the absorbance of the light in the medium. However, our observation shows that the particles experience smaller force (velocity) in water than in ethanol, while water has stronger absorption than ethanol.

In addition, the strong absorption of laser energy heats up the liquid, and the liquid molecules would move around and create fluidic convection. The particle motion may originate from the fluidic turbulence. To minimize the flow thus eliminate the flow induced force on the microparticles, we inserted a plastic plate inside the cuvette to isolate the left- and right- half of the cuvette, but kept the light passing through the plastic sheet. We also punched an opening (diameter 1 mm) on the plastic sheet to let the particles pass through in response to the PNJ mediated force (see schematics of the experimental process in Fig. 3a). The flow is minimized between left- and right- halves, as the particles will predominantly stay in respective halves of the cuvette with isolated turbulence between two halves. The dielectric microspheres are supplied in the right-hand side. In the presence of pulsed laser, the microsphere will be attracted to the light and enter the left-hand side (upstream) via the small opening, thus corroborating that the particle motion is due to the optical backaction force instead of the flow convection (Fig. 3b).

Interplay of light absorption and thermal conductivity

The optically mediated backaction force is the interplay of light absorption and thermal conductivity. We performed experiment in pure ethanol environment, and found that the optically induced backaction force was much stronger in pure ethanol. The optical backaction force at 1W power for 10 μm polystyrene sphere is ~400 pN(c.f., ~100 pN in water). The absorption coefficients of pure water and ethanol are experimentally measured to be $\gamma_w = 7.4\ cm^{-1}$ and $\gamma_{eth} = 5.0$ cm^{-1} respectively. The minute absorbance difference fails to explain the magnitude difference of force on particle in both media (Fig. 4a). Since the PNJ concentrates in an exhaustive environment, empirically, we define net absorption as the ratio of light absorption and the thermal conductivity, $\sigma = \gamma_{mix}/\kappa_{mix}$. The mixture of water and ethanol assumes a linear system, and the absorption coefficient approximates, $\gamma_{mix} = (1-c)\gamma_w + c\gamma_{eth}$, with c the volume fraction (concentration) of ethanol. Similarly, the thermal conductivity of the mixture can be estimated by $\kappa_{mix} = (1-c)\kappa_w + c\kappa_{eth}$, where $\kappa_w = 0.606\ W/(m \cdot K)$ and $\kappa_{eth} = 0.17\ W/(m \cdot K)$ are correspondingly the thermal conductivities of water and ethanol. The experiment was run in mixture of ethanol and water, and the particle speed approximately increases linearly with the net absorption (Fig. 4b).

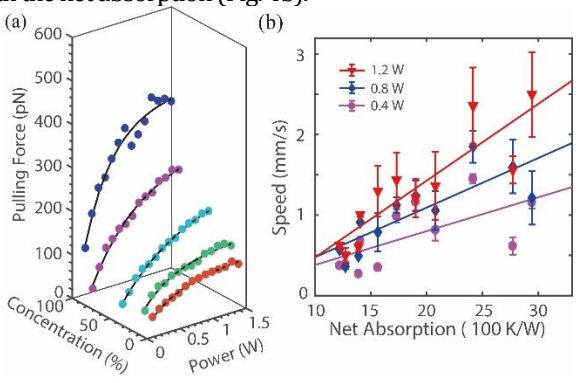

Figure 4. The pulling force increases significantly with the ethanol concentration but approximately scales linearly with the net absorption. (a), The force as function of power under multiple alcohol concentrations. (b), The increase of motion speed with net absorption at three power levels approximately suggests a linear relationship between the particle speed and the net absorption.

The linear relationship of the speed with respect to the net absorption suggests that the backaction is the competition of light absorption and the thermal conductivity. Such observation allows the control of the magnitude of backaction force by engineering the composition of background medium. In other words, the passive backaction force could be applied as a sensor for monitoring the physiological conditions to inspect the disease.

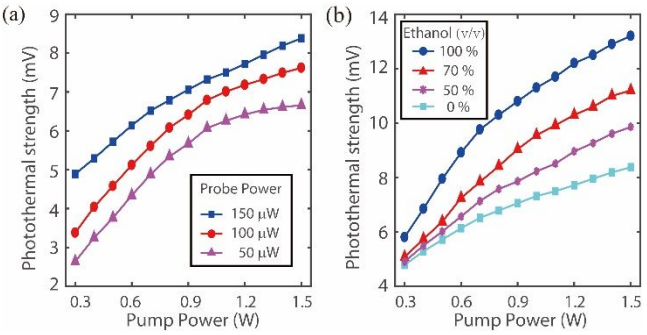

Figure 5. The photothermal strength increases with the alcohol concentration. (a), The benchmark test for the photothermal system shows increase of the photothermal signal magnitude with the probe beam power. (b), The thermal lens effect augments as the ethanol concentration increases. Shown are ethanol volume fractions of 0 % (cyan square), 50 % (magenta star), 75 % (red triangle), 100 % (blue circle). The probe beam powers are kept at 150 μW.

The monotonic increase of force with respect to power shows a saturation behavior (Fig. 4a). We show that this saturation attributes to the photothermal effect. According to Eq. (1), the force approximates, $F \propto \Delta T/\sqrt{T_0}$. Intuitively, as the suspension inherently absorbs the light energy, the local background temperature, T_0, thus the force (velocity) increases slower at high level of beam power than at a weak power. Such global temperature increase could induce a local refractive index gradient and a 'thermal lens'[28,39]. We identify this effect by monitoring the power fluctuation of a separate probe beam coaligned with the pulsed laser ('pump') (See Supplementary Materials). The pulsed pump beam was mechanically chopped with a certain frequency to alternately excite the thermal lens. The transmitted probe beam was locked in with the chopper frequency. In particular, we used a visible wavelength (633 nm) in the pump-probe configuration to detect the photothermal signal with high sensitivity photodetector. As the pump beam power increases, the photothermal signal increases monotonically with the pump power (Fig. 5a). In the mixture of ethanol and water, the photothermal effect is augmented with increase of ethanol concentration due to reduced thermal conductivity (Fig. 5b). This implies that the heat in ethanol exhausts to the environment more slowly, producing stronger 'thermal lens' effect. Thus, the alleviation of backaction force at high power level attributes to the global heating.

Microparticle classification with PNJ-mediated force

Biological cells have a refractive index greater than the surrounding medium, and can also form PNJ, which maintains a backaction force on the cell. Such biophotonic nanojet has been applied for nanoparticle manipulation and imaging[34,40]. We demonstrate that the biophotonic nanojet can also provide backaction force. This has been corroborated by the fact that the yeast cell moves towards the light source in the presence of light. As we alternate the laser beam, the average speed of the yeast cells keeps switching between two levels (Fig. 6a). The directional motion speed of the yeast cell also increases with the incident laser power (Fig. 6b). In particular, the PNJ provides large-scale cell manipulation as long as the cell is within the collimated beam under orthogonal microscopy, no matter the cells are in focus or out of focus (Fig. 6c), the cells all move towards the light source.

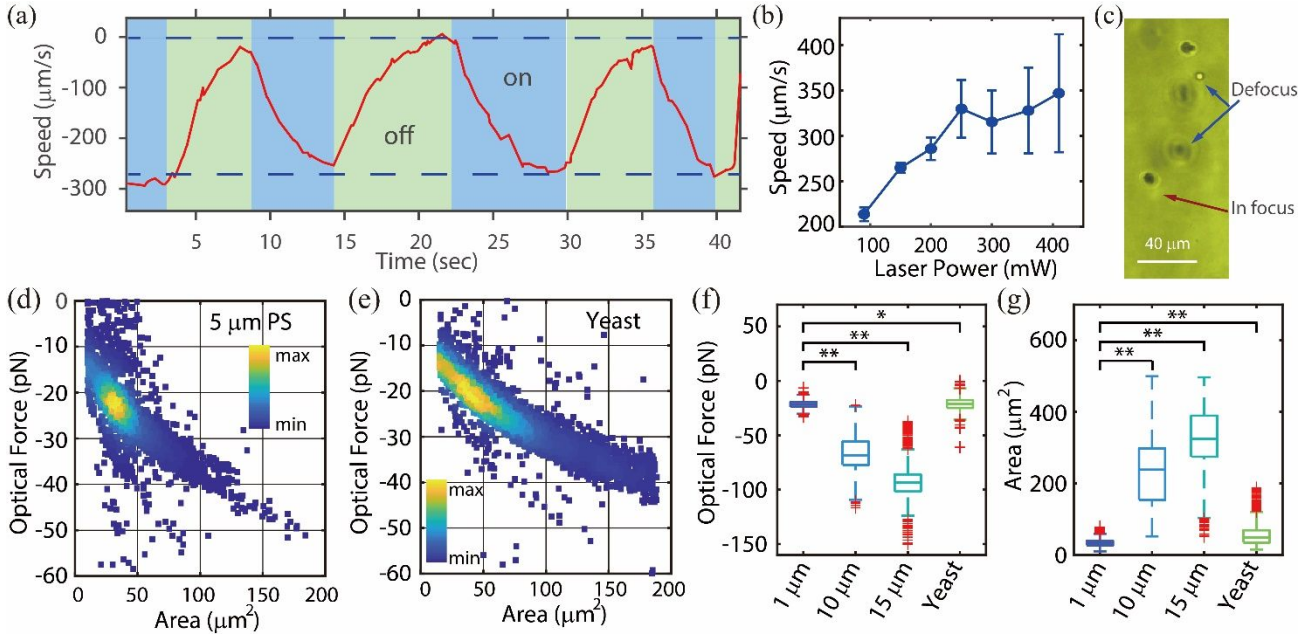

Figure 6. The optical pulling of biological cells. (a), the average speed of the yeast cells keeps switching between two levels under the alternating beam illumination. (b), the backaction speed on yeast cell increases with the injected laser power. (c), Microscopic image of yeast cells either in focus or out of focus. (d), The 5 μm polystyrene sphere and (e), the yeast cells form a homogeneous population. The color-coding represents a linear density population scale. Boxplots of the (f) optical force and (g) measured particle area for yeast cell as comparison with polystyrene spheres with various diameters. Statistical significance is determined by a paired *t*-test for each group; * $P<0.03$, ** $P<0.001$.

The backaction under PNJ works with collimated beam, which alleviates the phototoxicity on the biological cells. We elect to use an average power of 150 mW, which provides a power density of ~0.3 W/cm^2 comparable to that of sunlight to minimize photodamage. The detection objective was replaced by a large magnification objective to provide better resolution

(Olympus, 20x, NA=0.40). Both the size and the optical force of the particle were evaluated from the video microscopy. We run the experiment with polystyrene sphere of 5 μm diameter (comparable with the yeast cell), and the 2D occurrence histogram centered around the force of 22.8 ± 4.2 pN, and the area of 34.1 ± 12.2 μm^2 (N=31,712 microspheres for the population in Fig. 6d). The biological cells are of various types, and the physiological function of cells differs from cell types. The classification of the cell types has been an important scrutiny method to decide whether the cell is functioning normally or under sick condition. Existing cytometers including the fluorescence flow cytometer, the ultra-high-speed imaging, and the real-time deformability cytometry, rely on either the fluorescence or the cell morphology under microscope to classify cell types[41-43]. We demonstrate the application of the PNJ-mediated force to tackle this classical problem in cell biology and environmental sciences. The optical force on the yeast cell follow normal distribution, which suggests an average magnitude of force of 22.9 ± 6.3 pN, and the area of 57.5 ± 34.0 μm^2 (N= 10,032 yeast cells for the population in Fig. 6e) is on the same order of the reported diameter of yeast about 5~7 μm in the reference[44]. The refractive index of the yeast cell is 1.385, slightly above that for the background water[44]. The boxplots show the optical force (Fig. 6f) and area (Fig. 6g) for the yeast cells and polystyrene sphere of various sizes. A paired t-test evaluates the statistical significance with the probability * P<0.03 and ** P<0.001 to reject the null hypothesis. The size measurement also changes with the axial position and provides a guidance to the geometry of the microparticle. The motion trajectories of the yeast cell are random and part of them are outside the focal plane of the detection objective due to limited depth of field. For instance, the defocused yeast cell yields a measured size either greater or smaller than the actual size when the cell is out of focus (Fig. 6c). Therefore, the size measurement may deviate from the nominal size and varies across a broad range. This effect will augment as the particle size is much greater than the depth of field (5.8 μm for the 20x NA=0.40 Olympus objective). We corroborate the broadening of size range using polystyrene sphere with 10 μm and 15 μm diameter (over twice of the depth of field), and the experiment suggests an area of 230 ± 90 μm^2 (N= 5,531 for 10 μm) and 330 ± 84 μm^2 (N= 1,561 for 15 μm), the over estimation of size for larger particles attributes to the increased deviation for the defocused spheres. Moreover, the particle distribution scatters more rather than well centered at the point determined by the average force and area. This is mainly due to the fact that the captured image records the diffracted out-of-focus microsphere in presence of random Brownian motion and the uncertain axial position with respect to the detection microscopy. The comparison suggests that for the particle classification, the characteristic particle size should be smaller than or comparable to the depth of field of the detection microscopy, which sets the size range of particle classification. As the biological cells in the natural conditions often encounters mechanical stress, e.g., the red blood cell compressed by the vessel, the PNJ mediated force may induce additional deformation on the cell when it passes through narrow channels. The PNJ mediated force can be potentially applied in mechanobiology, such as the cell deformability and in general the membrane stiffness[41,45].

Conclusion

In conclusion, we have reported on a passive back-action force in dielectric microparticle suspension established by the PNJ. We have provided theoretical evidence for the back-action force and the size dependence, in excellent agreement with the experimental observation. Furthermore, as the laser power increases, the back-action force shows a saturation behavior which arises from the increase of temperature for the background medium owing to the photothermal effect. In contradistinction to the active back-action forces in artificial and natural creatures, the observed PNJ provides a passive back action system, which stems from the competition between light absorption and thermo-conductivity. Nevertheless, the particles do not need to be localized in narrow region (as compared with interferometric or resonant trapping schemes[15,16,24]), and allows large-scale manipulation of microparticles. Since the biological particles are mostly dielectric and fall in the size range of micrometers, our observation can be well extended to biophotonic applications using PNJ, such as cell classification and sorting. Moreover, backaction force also allows the collection and clearing of the dielectric particles, and micro-organisms in environmental water for pollution control.

Methods

Custom-built mode-locked fiber laser source

The custom-built mode-locked fiber laser consisted of a 0.5-m single-mode fiber (SMF, Corning, HI1060), 3.6-m lowly doped EDF (Levent-SFD), and 0.5-m standard SMF (Corning, SMF 28e). A single-mode optical integrated module (OIM) combining wavelength-division multiplexing (WDM), beam splitter, and polarization-sensitive isolator (P-ISO), couples the pump and extracts 50% of laser to the output. The EDF was pumped by a 976-nm single-mode laser diode (LD) [46]. Two in-line polarization controllers (PCs) manipulated the polarization state of light inside cavity. Combined manipulation of nonlinearity (i.e., self-phase modulation), dispersion, and polarization allows broadband operation. The direct output power was ~20 mW at a pump power of 120 mW. The laser pulse width was measured by an autocorrelator (Femtochrome, FR-103 MN) with a full-width-at-half-maximum of 1.6 ps. The optical spectrum was evaluated by sending the pulsed beam into an optical spectrum analyzer (OSA, Yokogawa AQ6375). Optical spectrum before the amplification demonstrates a 3-dB bandwidth of 53 nm (Fig. S2). The pulsed laser coupled out from the fiber laser loop has a maximum average power of 16 mW and was amplified by an L-band erbium-doped fiber amplifier (EDFA). Only the stronger portion of the original spectrum was amplified, producing pulsed beam with a central wavelength of 1576 nm, and a 3-dB spectral bandwidth of 18 nm and variable output from 0.3~2 W. The amplified temporal pulse train was

detected by a 10-GHz high speed photodetector (HiPD, HP 11982A), and was digitalized by a real time oscilloscope (Lecroy SDA 820Zi-B). The pulses have a repetition period of 22.5 ns corresponding to a repetition rate of 44.5 MHz (Fig. S2b). The amplified pulsed laser was coupled to free space via a fiber collimator. The collimated beam directly shines or is relayed by a telescope to shine on the cuvette with dielectric particle suspension.

Particle imaging, tracking, and photonic nanojet simulation

An LED (Thorlabs, M530L3), relayed by a lens (f=200 mm), provides bright-field illumination on the sample, orthogonal to the pulsed laser line. The particle motion behavior was monitored by video microscope through an objective lens (Olympus, 4x, NA=0.1) and a color CMOS camera (DC1645c-HQ, Thorlabs) (see supplementary Fig. S4). Depending on experiment, a 25 mm TV lens (Electrophysics TV lens) was assisted to alter the field of view. For yeast cell manipulation, the objective lens was replaced by higher magnification version (Olympus, 20x, NA=0.40). The images were digitalized at a speed of 25 fps and saved on local computer. Depending on the speed of microsphere, the camera can be configured at a higher speed up to ~120 fps with a reduced field of view. The particle positions were analyzed from the video series using the particle tracking algorithm[47]. We included morphology analysis to make the algorithm more robust for various types of particles and to extract the geometry of particles. The electromagnetic field distribution of the photonic nanojet was numerically calculated using Finite Difference Time Domain (FDTD) package in Lumerical (Lumerical Inc.) with plane wave illumination, while the temperature distribution near the nanojet was simulated using DEVICE module.

Sample preparation

All the testing reported were conducted with polystyrene microsphere (10 μm in diameter, F8833, ThermoFisher) except the size effect measurements. Polystyrene microsphere of various sizes (20 μm, 50 μm, 80 μm in diameter, Tianjin BaseLine Inc.) were suspended in deionized (DI) water (Millipore, 18.5 MΩ) for size-dependent research. Mixture of water and ethanol was prepared with a gradient ratio of the light absorption and thermal conductivity (net absorption), and the detailed recipe is summarized in Supplementary Table S1. The microsphere stock suspension was vortexed and sonicated before use to make sure that the microspheres are not aggregated and uniformly dispersed in the suspension. 50 μL of stock microsphere is suspended into 3 mL water for all the photothermal experiments. The yeast cell suspension was made by dissolving dry yeast in deionized water, and gently vortexed before the optical force experiment.

Thermal lens measurement

The photothermal effect was evaluated by sending a separate probe beam (wavelength 633 nm) coaligned with the picosecond pump beam. The pump beam was chopped by a mechanical chopper, the modulation frequency of which was fed into a lock-in amplifier. The probe beam power was monitored by a photodiode (Det10A2, Thorlabs) with the removal of the pump beam by a notch filter centered at 1550 nm wavelength. The transmitted probe beam was further collected by a lens (f=50 mm) onto the photodiode. The output from the photodiode was sent to custom-built lock-in amplifier synchronized at the chopper modulation frequency at low noise mode. The probe power was adjusted by a variable attenuator wheel (Thorlabs Inc.).

ASSOCIATED CONTENT

Supporting Information. This material is available free of charge via the Internet at http://pubs.acs.org." Optical force analysis, detailed experimental setup and sample preparation.

AUTHOR INFORMATION

Corresponding Author

*Email: C.Q. (chengwei.qiu@nus.edu.sg); K. T. (tsia@hku.hk); K. W. (kywong@eee.hku.hk)

Author Contributions

#Y.X. Ren, X. Zeng, and L. M. Zhou contributed equally to this work. K.W., C.-W. Q., Y.R. conceived the idea and supervised the whole project. Y.R., X.Z. and C.K. performed the research, analyzed the data. L.Z., Y. R. performed the theoretical analysis guided by C.-W. Q.. K.W., C.-W. Q., Y.R. wrote the manuscript with input from all authors. All authors discussed and revised the manuscript.

Funding Sources

Research Grants Council of the Hong Kong Special Administrative Region of China (HKU C7047-16G, HKU 17209018, E-HKU701/17, CityU T42-103/16-N, and HKU 17205215), and Natural Science Foundation of China (N_HKU712/16). C.-W. Q. acknowledges the support from Ministry of Education, Singapore (Grant No. R-263-000-D11-114).

Notes

The authors declare no competing financial interests.

ACKNOWLEDGMENT

The authors acknowledge financial support from Research Grants Council of the Hong Kong Special Administrative Region of China, and Natural Science Foundation of China.

REFERENCES

(1) Shvedov, V. G.; Rode, A. V.; Izdebskaya, Y. V.; Desyatnikov, A. S.; Krolikowski, W.; Kivshar, Y. S. Giant Optical Manipulation. *Physical Review Letters* **2010**, *105*, 118103.

(2) Ashkin, A.; Dziedzic, J. M.; Yamane, T. Optical trapping and manipulation of single cells using infrared laser beams. *Nature* **1987**, *330*, 769-771.

(3) Fazal, F. M.; Block, S. M. Optical tweezers study life under tension. *Nat Photon* **2011**, *5*, 318-321.

(4) Woodside, M. T.; Behnke-Parks, W. M.; Larizadeh, K.; Travers, K.; Herschlag, D.; Block, S. M. Nanomechanical measurements of the sequence-dependent folding landscapes of single nucleic acid hairpins. *Proceedings of the National Academy of Sciences* **2006**, *103*, 6190-6195.

(5) Horowitz, V. R.; Alemán, B. J.; Christle, D. J.; Cleland, A. N.; Awschalom, D. D. Electron spin resonance of nitrogen-vacancy centers in optically trapped nanodiamonds. *Proceedings of the National Academy of Sciences* **2012**, *109*, 13493-13497.

(6) Barredo, D.; Lienhard, V.; de Léséleuc, S.; Lahaye, T.; Browaeys, A. Synthetic three-dimensional atomic structures assembled atom by atom. *Nature* **2018**, *561*, 79-82.

(7) Kumar, A.; Wu, T.-Y.; Giraldo, F.; Weiss, D. S. Sorting ultracold atoms in a three-dimensional optical lattice in a realization of Maxwell's demon. *Nature* **2018**, *561*, 83-87.

(8) Zhou, L.-M.; Xiao, K.-W.; Chen, J.; Zhao, N. Optical levitation of nanodiamonds by doughnut beams in vacuum. *Laser & Photonics Reviews* **2017**, *11*, 1600284.

(9) Ashkin, A.; Dziedzic, J. M.; Bjorkholm, J. E.; Chu, S. Observation of a single-beam gradient force optical trap for dielectric particles. *Opt. Lett.* **1986**, *11*, 288-290.

(10) Ashkin, A.; Dziedzic, J. M. Optical Levitation by Radiation Pressure. *Applied Physics Letters* **1971**, *19*, 283-285.

(11) Shvedov, V.; Davoyan, A. R.; Hnatovsky, C.; Engheta, N.; Krolikowski, W. A long-range polarization-controlled optical tractor beam. *Nature Photonics* **2014**, *8*, 846.

(12) Kajorndejnukul, V.; Ding, W.; Sukhov, S.; Qiu, C.-W.; Dogariu, A. Linear momentum increase and negative optical forces at dielectric interface. *Nature Photonics* **2013**, *7*, 787.

(13) Chen, J.; Ng, J.; Lin, Z.; Chan, C. T. Optical pulling force. *Nature Photonics* **2011**, *5*, 531.

(14) Ruffner, D. B.; Grier, D. G. Optical Conveyors: A Class of Active Tractor Beams. *Physical Review Letters* **2012**, *109*, 163903.

(15) Dogariu, A.; Sukhov, S.; Sáenz, J. Optically induced "negative forces". *Nature Photonics* **2012**, *7*, 24.

(16) Descharmes, N.; Dharanipathy, U. P.; Diao, Z.; Tonin, M.; Houdré, R. Observation of Backaction and Self-Induced Trapping in a Planar Hollow Photonic Crystal Cavity. *Physical Review Letters* **2013**, *110*, 123601.

(17) Ding, W.; Zhu, T.; Zhou, L.-M.; Qiu, C.-W. Photonic tractor beams: a review. *Advanced Photonics* **2019**, *1*, 1-14.

(18) Qiu, C.-W.; Ding, W.; Mahdy, M. R. C.; Gao, D.; Zhang, T.; Cheong, F. C.; Dogariu, A.; Wang, Z.; Lim, C. T. Photon momentum transfer in inhomogeneous dielectric mixtures and induced tractor beams. *Light: Science & Applications* **2015**, *4*, e278.

(19) Taylor, M. A.; Waleed, M.; Stilgoe, A. B.; Rubinsztein-Dunlop, H.; Bowen, W. P. Enhanced optical trapping via structured scattering. *Nat Photon* **2015**, *9*, 669-673.

(20) Lee, S.-H.; Roichman, Y.; Grier, D. G. Optical solenoid beams. *Opt. Express* **2010**, *18*, 6988-6993.

(21) Grier, D. G. A revolution in optical manipulation. *Nature* **2003**, *424*, 810-816.

(22) Lu, J.; Li, Q.; Qiu, C.-W.; Hong, Y.; Ghosh, P.; Qiu, M. Nanoscale Lamb wave–driven motors in nonliquid environments. *Science Advances* **2019**, *5*, eaau8271.

(23) Lu, J.; Yang, H.; Zhou, L.; Yang, Y.; Luo, S.; Li, Q.; Qiu, M. Light-Induced Pulling and Pushing by the Synergic Effect of Optical Force and Photophoretic Force. *Physical Review Letters* **2017**, *118*, 043601.

(24) Juan, M. L.; Gordon, R.; Pang, Y.; Eftekhari, F.; Quidant, R. Self-induced back-action optical trapping of dielectric nanoparticles. *Nature Physics* **2009**, *5*, 915.

(25) Novitsky, A.; Qiu, C.-W.; Wang, H. Single Gradientless Light Beam Drags Particles as Tractor Beams. *Physical Review Letters* **2011**, *107*, 203601.

(26) Brzobohatý, O.; Karásek, V.; Šiler, M.; Chvátal, L.; Čižmár, T.; Zemánek, P. Experimental demonstration of optical transport, sorting and self-arrangement using a 'tractor beam'. *Nature Photonics* **2013**, *7*, 123.

(27) Phuoc, T. X. A comparative study of the photon pressure force, the photophoretic force, and the adhesion van der Waals force. *Optics Communications* **2005**, *245*, 27-35.

(28) Horvath, H. Photophoresis – a Forgotten Force ?? *KONA Powder and Particle Journal* **2014**, *31*, 181-199.

(29) Ashkin, A.; Dziedzic, J. M. Optical trapping and manipulation of viruses and bacteria. *Science* **1987**, *235*, 1517-1520.

(30) Luk'yanchuk, B. S.; Paniagua-Domínguez, R.; Minin, I.; Minin, O.; Wang, Z. Refractive index less than two: photonic nanojets yesterday, today and tomorrow [Invited]. *Opt. Mater. Express* **2017**, *7*, 1820-1847.

(31) Wang, Z.; Guo, W.; Li, L.; Luk'yanchuk, B.; Khan, A.; Liu, Z.; Chen, Z.; Hong, M. Optical virtual imaging at 50 nm lateral resolution with a white-light nanoscope. *Nature Communications* **2011**, *2*, 218.

(32) Heifetz, A.; Kong, S.-C.; Sahakian, A. V.; Taflove, A.; Backman, V. Photonic Nanojets. *Journal of Computational and Theoretical Nanoscience* **2009**, *6*, 1979-1992.

(33) Chen, Z.; Taflove, A.; Backman, V. Photonic nanojet enhancement of backscattering of light by nanoparticles: a potential novel visible-light ultramicroscopy technique. *Opt. Express* **2004**, *12*, 1214-1220.

(34) Li, Y.-C.; Xin, H.-B.; Lei, H.-X.; Liu, L.-L.; Li, Y.-Z.; Zhang, Y.; Li, B.-J. Manipulation and detection of single nanoparticles and biomolecules by a photonic nanojet. *Light: Science & Applications* **2016**, *5*, e16176-e16176.

(35) Born, B.; Krupa, J. D. A.; Geoffroy-Gagnon, S.; Holzman, J. F. Integration of photonic nanojets and semiconductor nanoparticles for enhanced all-optical switching. *Nature Communications* **2015**, *6*, 8097.

(36) Lee, J. Y.; Hong, B. H.; Kim, W. Y.; Min, S. K.; Kim, Y.; Jouravlev, M. V.; Bose, R.; Kim, K. S.; Hwang, I.-C.; Kaufman, L. J.; Wong, C. W.; Kim, P.; Kim, K. S. Near-field focusing and magnification through self-assembled nanoscale spherical lenses. *Nature* **2009**, *460*, 498-501.

(37) Wang, F.; Liu, L.; Yu, H.; Wen, Y.; Yu, P.; Liu, Z.; Wang, Y.; Li, W. J. Scanning superlens microscopy for non-invasive large field-of-view visible light nanoscale imaging. *Nature Communications* **2016**, *7*, 13748.

(38) Ren, Y.-X.; Wu, J.; Lai, Q. T. K.; Lai, H. M.; Siu, D. M. D.; Wu, W.; Wong, K. K. Y.; Tsia, K. K. Parallelized volumetric fluorescence microscopy with a reconfigurable coded incoherent light-sheet array. *Light: Science & Applications* **2020**, *9*, 8.

(39) Lamhot, Y.; Barak, A.; Peleg, O.; Segev, M. Self-Trapping of Optical Beams through Thermophoresis. *Physical Review Letters* **2010**, *105*, 163906.

(40) Li, Y.; Liu, X.; Li, B. Single-cell biomagnifier for optical nanoscopes and nanotweezers. *Light: Science & Applications* **2019**, *8*, 61.

(41) Rosendahl, P.; Plak, K.; Jacobi, A.; Kraeter, M.; Toepfner, N.; Otto, O.; Herold, C.; Winzi, M.; Herbig, M.; Ge, Y.; Girardo, S.; Wagner, K.; Baum, B.; Guck, J. Real-time fluorescence and deformability cytometry. *Nature Methods* **2018**, *15*, 355-358.

(42) Santos-Ferreira, T.; Herbig, M.; Otto, O.; Carido, M.; Karl, M. O.; Michalakis, S.; Guck, J.; Ader, M. Morpho-Rheological Fingerprinting of Rod Photoreceptors Using

Real-Time Deformability Cytometry. *Cytometry Part A* **2019**, *95*, 1145-1157.

(43) Lee, K. C. M.; Wang, M.; Cheah, K. S. E.; Chan, G. C. F.; So, H. K. H.; Wong, K. K. Y.; Tsia, K. K. Quantitative Phase Imaging Flow Cytometry for Ultra-Large-Scale Single-Cell Biophysical Phenotyping. *Cytometry Part A* **2019**, *95*, 510-520.

(44) Müller, D.; Glöckler, F.; Kienle, A. Application of Mie theory for enhanced size determination of microparticles using optical particle counters. *Applied Optics* **2019**, *58*, 4575-4584.

(45) Bashant, K. R.; Vassallo, A.; Herold, C.; Berner, R.; Menschner, L.; Subburayalu, J.; Kaplan, M. J.; Summers, C.; Guck, J.; Chilvers, E. R.; Toepfner, N. Real-time deformability cytometry reveals sequential contraction and expansion during neutrophil priming. *Journal of Leukocyte Biology* **2019**, *105*, 1143-1153.

(46) Kang, J.; Feng, P.; Wei, X.; Lam, E. Y.; Tsia, K. K.; Wong, K. K. Y. 102-nm, 44.5-MHz inertial-free swept source by mode-locked fiber laser and time stretch technique for optical coherence tomography. *Opt. Express* **2018**, *26*, 4370-4381.

(47) Kelley, D. H.; Ouellette, N. T. Using particle tracking to measure flow instabilities in an undergraduate laboratory experiment. *American Journal of Physics* **2011**, *79*, 267-273.

For Table of Contents Use Only.

Photonic nanojet mediated backaction of dielectric microparticles

Yu-Xuan Ren, Xinglin Zeng, Lei-Ming Zhou, Cihang Kong, Huade Mao, Cheng-Wei Qiu, Kevin K. Tsia, Kenneth K. Y. Wong

Spherical microparticles focus light into subdiffraction-limited photonic nanojet (PNJ) with extreme intensity. Such PNJ is able to heat up the local surrounding molecules, leading to thermal expansion within the narrow region. In return, the molecular expansion pushes the microparticle backwards with a 'negative optical force'. We have observed such phenomenon in purely dielectric photothermal system, and the mechanism is attributed to the competing effect between the absorption and the thermal conductivity of the surrounding medium. In combination with the morphology analysis, the optical force can be applied to classify microparticles, e.g., the polymer sphere and biological cells.